

## Article

# Enhanced Power Factor Correction and Torque Ripple Mitigation for DC–DC Converter Based BLDC Drive

Geethu Krishnan <sup>1,2,3,4</sup> , Moshe Sitbon <sup>1,\*</sup>  and Shijoh Vellayikot <sup>2,3</sup> 

<sup>1</sup> Department of Electrical and Electronic Engineering, Ariel University, Ariel 40700, Israel; geethuk@ariel.ac.il

<sup>2</sup> Department of Electrical and Electronic Engineering, Jyothi Engineering College, Thrissur 679531, Kerala, India; shijohv@jecc.ac.in

<sup>3</sup> CET Campus, APJ Abdul Kalam Technological University, Thiruvananthapuram 695016, Kerala, India

<sup>4</sup> Department of Electrical and Electronic Engineering, Carmel College of Engineering and Technology, Alappuzha 688004, Kerala, India

\* Correspondence: moshesi@ariel.ac.il

**Abstract:** A novel approach to the design of power factor correction (PFC) and torque ripple minimization in a brushless direct current (BLDC) motor drive with a new pulse width modulation (PWM) technique is demonstrated. The drive was designed to have a better power factor (PF) and less torque ripple. On the other hand, the modified Zeta converter is used to enhance the power factor of the proposed system. The modified Zeta converter is operated in discontinuous inductor current mode (DICM) by using a voltage follower technique, which only needs a voltage sensor for power factor correction (PFC) operation and DC-link voltage control. The output voltage of the VSI is determined by switching patterns generated by the PWM-ON-PWM switching strategy, and it reduces the torque ripples. The proposed drive is developed and simulated in a MATLAB/Simulink environment. The power factor of 0.9999 is produced by the PFC modified zeta converter topology and the PWM-ON-PWM scheme reduce the torque ripple in the commutation region by 34.2% as compared with the PWM-ON scheme. This demonstrates the effectiveness of the suggested control method.



**Citation:** Krishnan, G.; Sitbon, M.; Vellayikot, S. Enhanced Power Factor Correction and Torque Ripple Mitigation for DC–DC Converter Based BLDC Drive. *Electronics* **2023**, *12*, 3533. <https://doi.org/10.3390/electronics12163533>

Academic Editors: Jianguo Zhu and Carlos Andrés García-Vázquez

Received: 11 June 2023

Revised: 13 August 2023

Accepted: 16 August 2023

Published: 21 August 2023



**Copyright:** © 2023 by the authors. Licensee MDPI, Basel, Switzerland. This article is an open access article distributed under the terms and conditions of the Creative Commons Attribution (CC BY) license (<https://creativecommons.org/licenses/by/4.0/>).

**Keywords:** power factor correction; torque ripples; BLDC; PWM-ON-PWM; zeta converter

## 1. Introduction

The BLDC motor's excellent efficiency, high energy density, high torque/inertia ratio, low maintenance requirements, and broad range of speed control make it the perfect motor for low and medium power applications [1]. The motor is a three-phase synchronous motor with permanent magnets on the rotor and three phase windings on the stator. There are no mechanical brushes or commutator assemblies, so it is sometimes called an electronically commutated motor. In BLDC motors, the rotor position is sensed by using hall effect sensors to provide electronic commutation [2,3]. Good power quality converters are required to achieve the unity power factor at AC mains with minimum current distortion [4,5]. In a conventional diode bridge rectifier (DBR) and high-value DC-link capacitor-provided BLDC motor driving system, a sizeable amount of harmonic current is pulled from the AC mains. Due to the integration of these elements, the supply current is severely distorted, resulting in a low PF at the AC mains and a current waveform with distinct peaks [6]. To power the BLDC motor drive, numerous single-phase power factor correction (PFC) converters have been described in the literature. A commonly employed approach involves the utilization of two-stage PFC converters, which employ two distinct converters for power factor correction and control of the DC-link voltage [7]. According to the type of application and the voltage level necessary for that specific application, a boost converter is typically employed as the first stage for PFC, followed by a second stage [8]. Two-stage power factor correction converters require larger numbers of MOSFET switches than single-stage power factor correction converters, which produce higher losses. Additionally, the

PFC and DC–DC conversion stage requires two different controllers, which raises the cost and complexity of the system. As their name implies, single-stage power factor correction converters need just one converter to handle both voltage control and the power factor correction function. Using a PFC boost converter is the most traditional method of fueling the BLDC motor. The BLDC motor’s voltage source inverter (VSI) keeps the DC-link voltage at the DC-link capacitor constant. Speed control is achieved via the pulse width modulation (PWM)-based switching of VSI, which has significant switching losses corresponding to the PWM switching frequency. Reference [9] makes a novel suggestion for changeable DC-link voltage for BLDC motor speed control. A comparison of permanent magnet synchronous motors and trapezoidal back emf BLDC motors reveals various advantages of the BLDC motors. These benefits include the capacity to function at high speeds, excellent reliability, and few maintenance needs. The torque ripple that occurs in the conduction and commutation zone of BLDC motors, which reduces BLDC drive precision, is their main flaw. Electric vehicles, robots, and industrial automation are just a few of the many applications in which BLDC drives are employed. But BLDC drives frequently have low power factors, which can decrease efficiency and put more strain on the power supply. Power factor correction is a method of raising the power factor of a load, usually by lowering the amount of reactive power required from the power source. For BLDC drives, a number of PFC methods have been suggested, including boost converters, buck-boost converters, and Sepic converters. However, these converters have some drawbacks, including difficult input current regulation and significant voltage stress on the switches. The buck-boost and the Sepic converter’s capabilities are combined in the DC–DC converter, which is known as the Zeta. It allows the input current to be regulated independently of the input voltage and has two inductors and two capacitors. Due to its ability to regulate the input current, it is in phase with the input voltage. This paper uses a Zeta converter to obtain a better power factor [10].

In [11], a voltage source inverter and a new control approach were used to obtain the commutation. For smooth electromagnetic torque, a phase current with a rectangular shape is ideal. Due to the armature winding inductance, a perfect rectangular phase current cannot be achieved. The inductance causes different slew rates for the two incoming and outgoing phases, which causes current ripples. The current ripples damage the electromagnetic torque and can produce mechanical vibration and noise [12]. To overcome these restrictions, a variety of complex and high-cost pulse width modulation approaches were proposed in [13]. There are reports that the switching losses and harmonics in front of the VSI unit can be reduced using unipolar and bipolar PWM approaches [14]. Therefore, throughout the operation, diode freewheeling and the commutation current ripple remained ignored. For the PFC, a topology based on a Luo converter installed before the standard BLDC motor drive using traditional PWM was created in [15]. The main issue with this topology is the current ripple caused by commutation, along with the fact that freewheeling of the inactive phase of the diode is not taken into account. The current and torque ripples in BLDC motor drives were addressed by the introduction of the ON-PWM method [16].

The commutation torque ripple under conventional two-phase operation is analyzed using a vector coordinate approach and provides a unique BLDCM drive method with vector control to reduce commutation torque ripple based on the analysis. This technique avoids switching the control method between the normal conduction period and the commutation period and increases system reliability by calculating the constraint equation of both torque ripple minimization and maximum torque per ampere characteristics [17]. It should be observed that at about 28%, the torque ripple is effectively reduced. Before the traditional BLDC motor drive, a super-lift Luo converter was utilized to handle current ripple for high-speed applications [18]. To suppress the commutation current ripple, a traditional SEPIC converter-based BLDC motor drive was used [19]. In [20], a notch filter was used to control unwanted AC components present in the DC link voltage across the capacitor of the DC–DC converter. The number of transistor switches increases size, switching losses, and complexity, and decreases the system’s efficiency. Therefore, to avoid

these restrictions, a single traditional SEPIC converter was used [21]. In [22], torque ripple was effectively reduced at about 28%, where copper losses and torque pulsations were somewhat reduced by using the dq-Transformation. In [23], torque ripples due to the diode free-wheeling of the inactive phase were considered, and were suppressed by nearly 32.5% using the PWM-Model Antiseptic Control Technique.

#### Contributions

The major contributions to this work are as follows:

- A modified zeta converter was used to improve the power factor and provide the DC link voltage to the voltage source inverter;
- Reducing the current and torque ripples during the commutation zone was given top priority in the current investigation, and duty cycle was also calculated;
- The effect of PWM-ON-PWM scheme on torque ripple minimization was examined;
- This neoteric method reduced the torque ripples and improved the power factor;
- The proposed control strategy was implemented using MATLAB/Simulink.

## 2. Problem Definition

Torque ripples in BLDC motors are mainly brought on by commutation torque ripple and diode freewheeling in the inactive period. These torque ripples can result in machine vibration when BLDC motors are employed in applications like underwater defense, potentially revealing the presence of the BLDC motor to adversaries. Therefore, it is crucial to reduce torque ripples in order for a BLDC motor to operate quietly and without vibration. To mitigate torque ripple arising from commutation, the PWM-ON-PWM scheme was implemented.

The diode bridge rectifier alone can create significant harmonic distortion and reduce the efficiency of the motor. The BLDC motor drive's power factor may be enhanced with the use of an improved zeta converter. Adding an improved zeta converter can correct the power factor by shaping the input current waveform and reducing the harmonic distortion. The zeta converter can smooth out the input current waveform, provide the motor with a more stable DC voltage, and reduce stress on the components. By improving the power factor and reducing the input current ripple, the zeta converter can increase the overall efficiency of the BLDC motor drive system. Energy savings and lower running costs may result from this.

## 3. Constructional Elements of BLDC Motor

Three stator windings and a rotor equipped with permanent magnets were used to develop the BLDC motor. A three-phase voltage source inverter provides power to the BLDC motor, with the motor being star-connected. The configuration is illustrated in Figure 1, where  $V_a$ ,  $V_b$ , and  $V_c$  represent the phase voltages and  $i_a$ ,  $i_b$ , and  $i_c$  denote the phase currents. Additionally,  $e_a$ ,  $e_b$ , and  $e_c$  represent the back emf;  $R$  represents the resistance per phase; and  $L$  represents the self-inductance per phase. The three-phase windings' voltage equations were:

$$\begin{cases} V_a = Ri_a + L \frac{di_a}{dt} + e_a + U_n \\ V_b = Ri_b + L \frac{di_b}{dt} + e_b + U_n \\ V_c = Ri_c + L \frac{di_c}{dt} + e_c + U_n \end{cases} \quad (1)$$

The electromagnetic torque is given by

$$T_e = \frac{e_a i_a + e_b i_b + e_c i_c}{\omega} \quad (2)$$

where  $\omega$  is the mechanical angular velocity of the rotor.

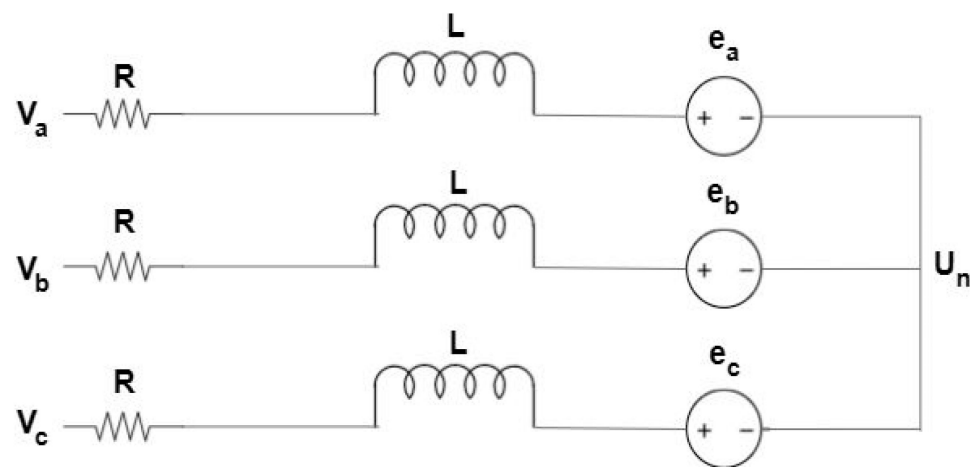


**Figure 1.** Equivalent circuit of BLDC motor.

In BLDC, the shape of the back emf is trapezoidal. There are six alternative rotor alignments  $60^\circ$  apart. This means that two phases commutate at a time, and the control, called the trapezoidal control, causes the rotor to spin. The hall sensors can determine the rotor's position to properly commutate the motor at the appropriate times with the appropriate phases. Commutation occurs in this manner. The rotor chases the stator's magnetic field rather than ever aligning with it. The motor of the BLDC engine requires a continuous voltage supplied by its three-phase converter to run continuously. However, the variable voltage must be used in order to drive the BLDC motor at various speeds. PWM logic can be used to accomplish this. Due to the inductance of the winding, the phase current of BLDC motors trails the phase voltage by an angle that depends on speed. This angle is greater if the BLDC motor is operating at a high speed. The phase voltage should be applied ahead of the phase current to the back-emf in order to generate the most torque. Any phase difference between the back-emf and phase current causes flux weakening, reduced torque, and low efficiency. A high state is produced when the rotor's north pole passes through a hall sensor, and a low state is produced when the south pole does so. When exposed to any  $60^\circ$  electrical arc, the three hall sensors produce three states of the signal, as shown in Figure 2. Six states are produced by the three hall sensors depending on the rotor's position. The controller will determine the two stator windings that need replacing based on the hall sensors' six states. The commutation is consequently continuous. Every  $60$  degrees of rotation, a DC voltage that is electrically switched energizes each phase terminal of the BLDC motor. As a result, each phase winding's waveform resembles a staircase with a step angle of  $60^\circ$  [24].

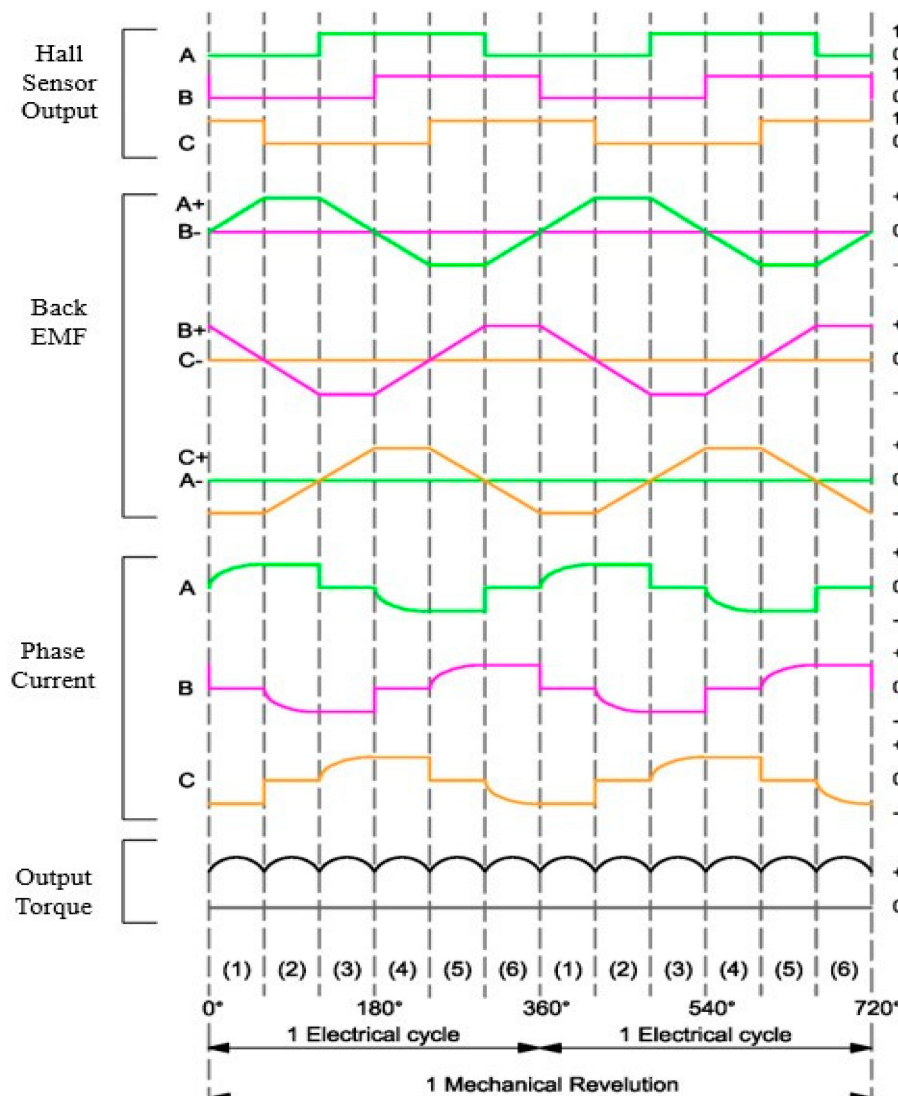


**Figure 2.** Hall sensor signal, back-emf, output torque, and phase current.

#### 4. Configuration of Proposed System

A detailed schematic of the proposed improved zeta converter-fed BLDC motor is shown in Figure 3. This arrangement uses a single-phase voltage source to convert the sinusoidal alternating current into a pulsing direct current using an uncontrolled semiconductor diode bridge rectifier. The action of full-wave rectification causes ripples in this pulsating DC voltage source. To provide a steady DC supply with reduced ripple factor, an LC filter was implemented, where  $L_f$  represents the filter inductance and  $C_f$  denotes the filter capacitance. The input of the modified zeta converter received this filtered DC supply. The modified zeta converter was made up of a PWM-controlled MOSFET switch  $S_w$ , input inductor  $L_i$ , output inductor  $L_o$ , intermediate capacitor  $C_i$ , and dc link capacitor  $C_d$ . The input inductor, intermediate capacitor, and output inductor all began charging when the MOSFET switch,  $S_w$ , was turned ON. The diode was in non-conduction mode during this time, since it was configured to be reverse-biased. The associated  $C_d$  was applied to the load. The diode transformed into a forward biased intermediate capacitor as soon as the switch was turned off, and the DC link capacitor discharged to the lower voltage. In this approach, the  $V_{Cd}$  or  $U_d$  of the modified Zeta converter was managed by a single voltage loop.

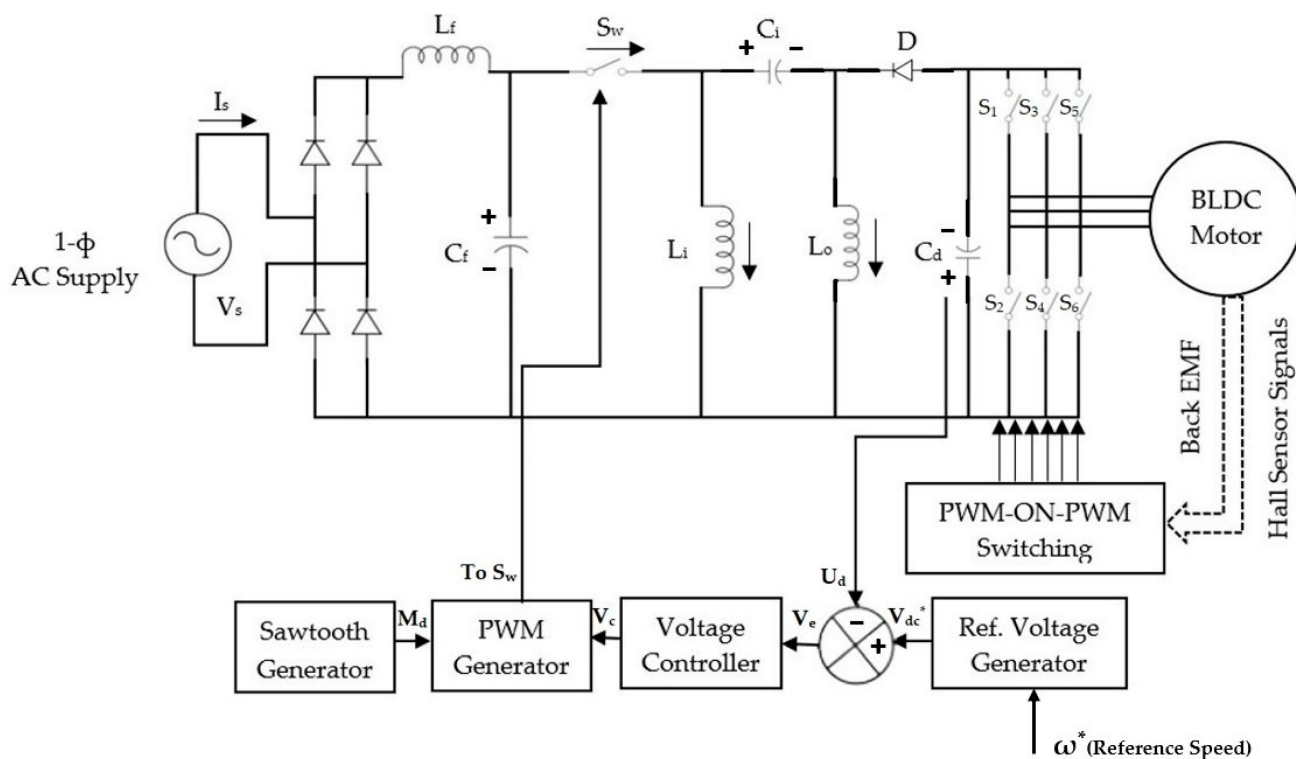


**Figure 3.** Modified zeta converter-fed BLDC drive.

A voltage source inverter (VSI) received the DC link voltage as a power source. A three-legged semiconductor switch-based bridge known as a VSI was designed. In the VSI design configuration, six MOSFET-based switches were employed. According to the diagram,  $S_1$ ,  $S_3$ , and  $S_5$  made up the upper legs, and  $S_2$ ,  $S_4$ , and  $S_6$  comprised the corresponding lower legs. The switching order was used to assign numbers to the switches.  $S_1$  was switched ON first, followed by  $S_2$ , then  $S_3$  was triggered ON after  $S_2$ . There was a  $60^\circ$  pause before each switch. The first leg was made up of  $S_1$  and  $S_2$ , and one phase of a three-phase output supply was given at their common junction point. The other two phases came from the following two legs. There were two toggle switches per leg. The lower switch was required to be OFF if the corresponding upper switch was ON, and vice versa. A positive half cycle of the corresponding phase was delivered to the load when the upper switch was ON and the lower switch was OFF. The opposite was required for the negative half cycle. In the same way, the subsequent upper and lower switches were actuated, with a gap of a  $120^\circ$  phase shift. With a  $2\pi/3$  phase shift between any two phases, a three-phase output voltage supply was achieved in this way. The three-phase stator winding of the BLDC motor received the three-phase output supply generated by the VSI in order to deliver the required flux. A speed encoder was used to measure the speed of the BLDC motor. The error signal was produced after comparing the actual speed to the reference speed. The PI controller's proportional and integral (PI) gain was used to amplify the error signal. Six switches were given the PWM-ON-PWM pulses to regulate their ON and OFF times. In this manner, PWM-ON-PWM managed the VSI's generated three-phase voltage, which in turn managed the speed of the BLDC motor. Block diagrams of the suggested model are depicted in Figure 4.

To reduce torque ripples in BLDC motors, the suggested strategy primarily chooses to use the PWM\_ON\_PWM scheme to send gate pulses to the inverter section. It is a bilateral modulation system in which the first and last  $30^\circ$  are in PWM mode, and the middle  $60^\circ$  are in constant turn-on mode, which is exhibited by switches of VSI and is shown in Figure 5. In this manner, the torque ripple brought on by the commutation current during the commutation period can be compensated for.

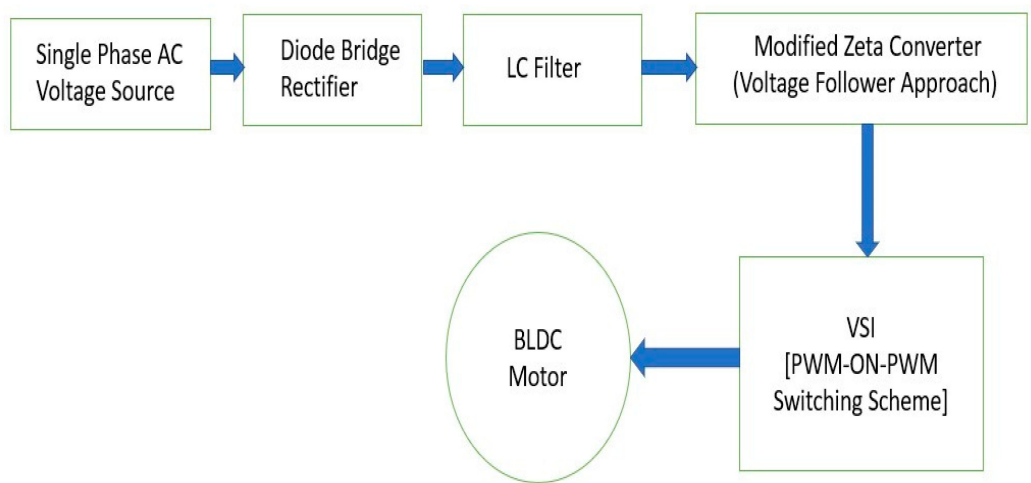


**Figure 4.** Block diagram of the proposed model.

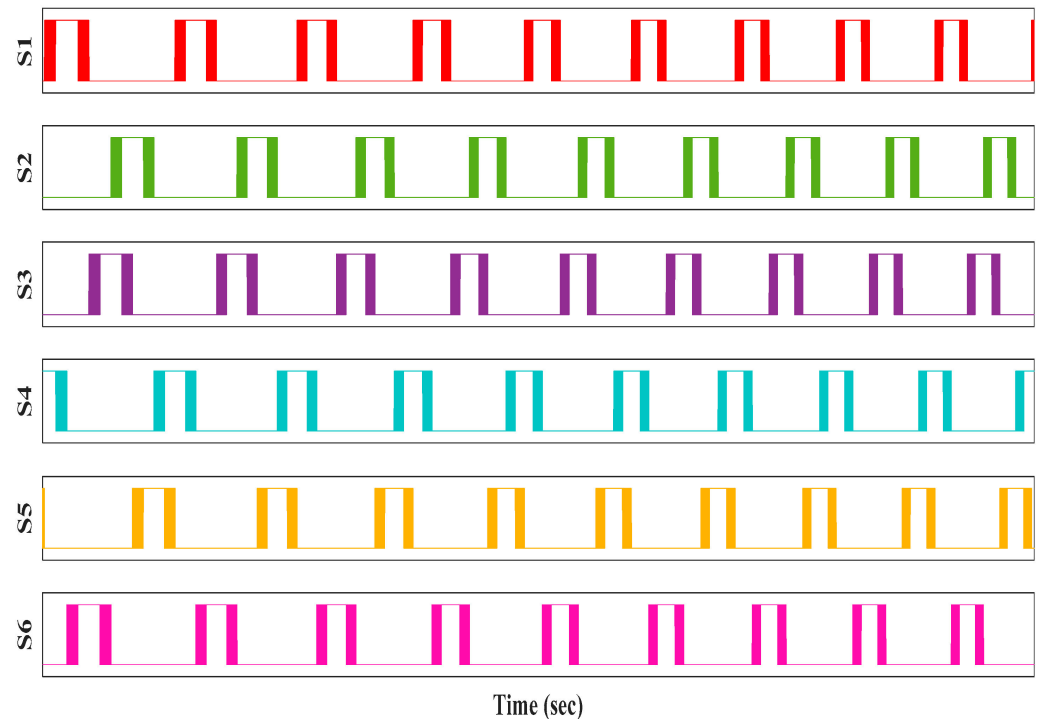


**Figure 5.** PWM-ON-PWM Pattern.

## 5. Operation of the Improved Zeta Converter

Figure 6 shows the basic circuit of the improved zeta converter. To increase the power factor of the BLDC motor drive, the improved zeta converter ran on discontinuous inductor current mode. In DICM, the current flow to the output inductor was not continuous in a cycle. In order for the PFC zeta converter to operate in DICM, the input side inductor ( $I_{L_i}$ ) needed to become discontinuous while the output side inductor ( $I_{L_o}$ ) and intermediate capacitor ( $V_{C_i}$ ) maintained continuous conduction during the switching cycle. In an entire switching cycle, the modified zeta converter could operate in four different modes. The modes of operation are explained below.

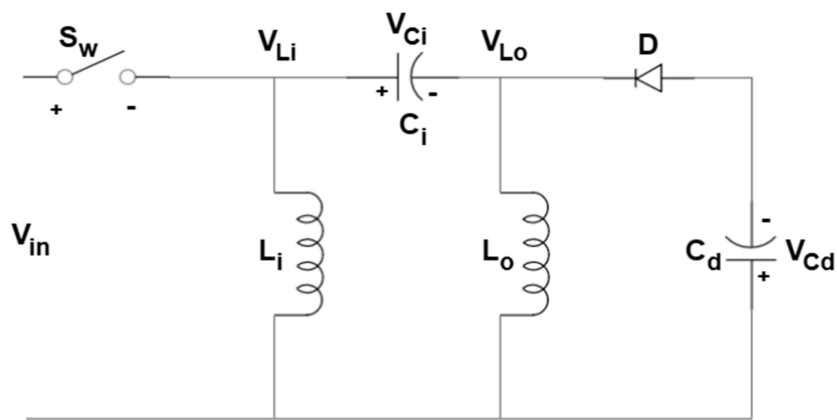


**Figure 6.** Basic circuit of zeta converter.

#### Mode 1

The Switch  $S_w$  must be turned on to enter this mode. Figure 7 illustrates how the charge begins to accumulate as soon as the switch is turned ON across the intermediate capacitor  $C_i$ , input inductor  $L_i$ , and output inductor  $L_o$ . The first mode is split into two parts. Due to the intermediate capacitor's negative charge in the first section, the voltage rises across it. In this mode, the  $C_d$  is directly loaded, while diode  $D$  is reverse-biased. In this mode, the DC link capacitor voltage dissipates via the load. Figure 7 illustrates how the intermediate capacitor begins to charge up in a positive way during the second phase of mode 1. This mode's output inductor current duration and intermediate capacitor voltage ( $C_i$ ) depend on the duty ratio.

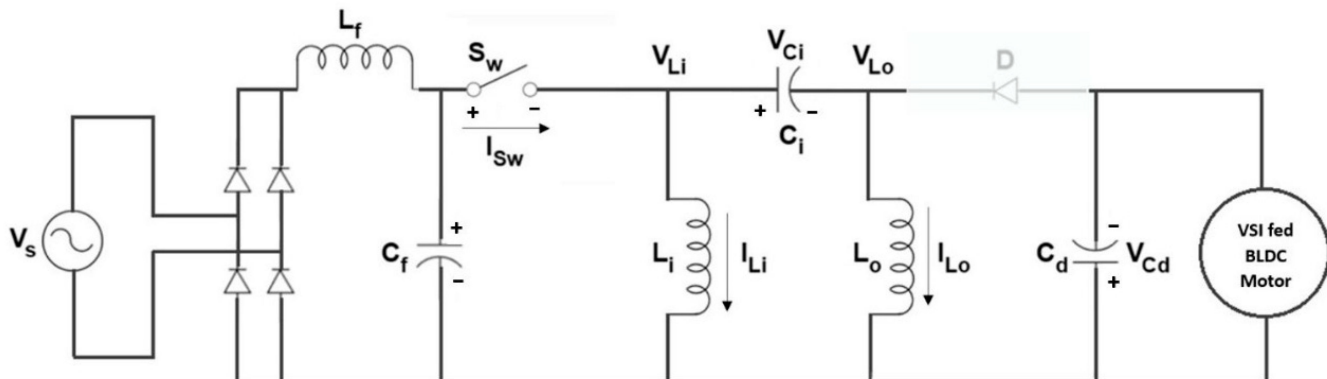


**Figure 7.** Mode 1 of the improved zeta converter.

#### Mode 2

The switch  $S_w$  should be turned off to enter this mode.  $C_i$  discharges in this manner in accordance with Figure 8. The output inductor current falls and the input inductor current increases as the intermediate capacitor voltage rises. When the diode  $D$  is forward-biased, it begins to conduct. Through this diode, the DC link capacitor charges, starting to increase the voltage across it. Figure 8 demonstrates that the diode current ( $I_D$ ) is produced by adding the input inductor current ( $I_{Li}$ ) and the output inductor current ( $I_{Lo}$ ) together. When the DC link capacitor reaches a voltage equal to the intermediate capacitor voltage  $V_{Ci}$ , this mode is terminated.

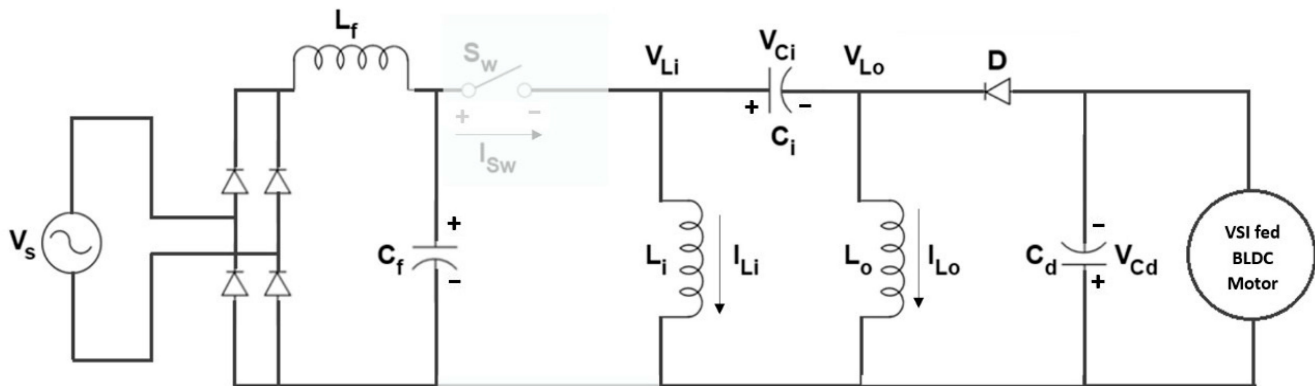


**Figure 8.** Mode 2 of the improved zeta converter.

### Mode 3

When  $V_{Ci}$  decreases from  $U_d$  and the intermediate capacitor continues to discharge between the input and output inductors, this mode starts. In this mode, the output inductor discharges through the forward-biased diode when the dc link voltage rises as a result of the dc link capacitor charging. As the current through the output inductor declines and the current through the input inductor increases, the voltage across the dc link capacitor increases. The output inductor's current decreases to zero in mode 3, since the modified Zeta converter is designed to operate in discontinuous inductor current mode. Because the output inductor is meant to be completely discharged, it must have a lower value than the input inductance. In Figure 9, Mode 3 is presented.

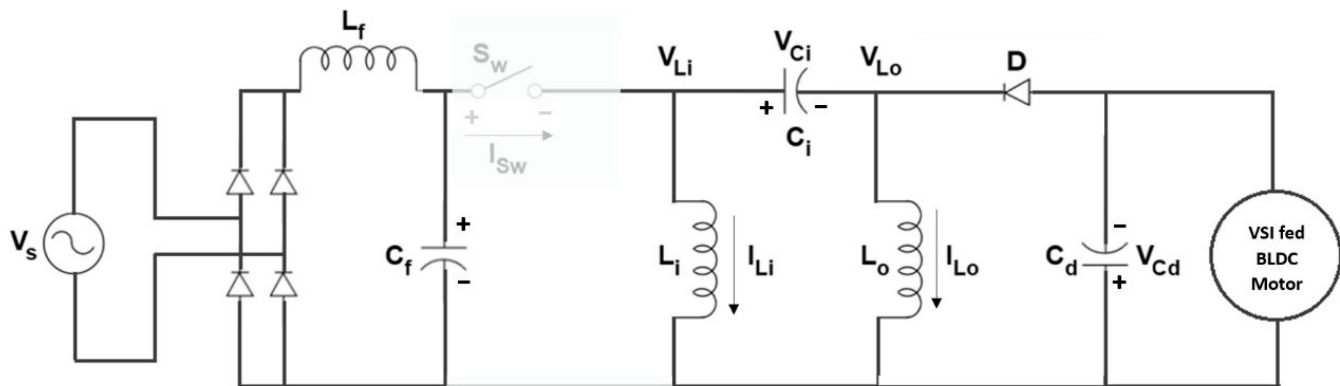


**Figure 9.** Mode 3 of the improved zeta converter.

### Mode 4

When reaching zero, the output inductor current reverses polarity to begin this mode. The two sections of this mode are also separated. The current rises in the initial portion of the mode input inductor as the intermediate capacitor keeps discharging. The output inductor current is equal to the inductor current during that time, since the diode is reverse-biased. As the  $C_d$  discharges through the load directly, the  $U_d$  becomes smaller. When the intermediate capacitor voltage reaches zero, the second phase of the mode begins. The intermediate capacitor then begins to charge with reverse polarity. Figure 10 illustrates the input inductor current used to charge  $C_i$  as the input inductor voltage decreased. Often, the duration of Mode 4 is the longest of all modes of operation. Switch  $S_w$  is then turned ON once more, and the cycle starts all over again.

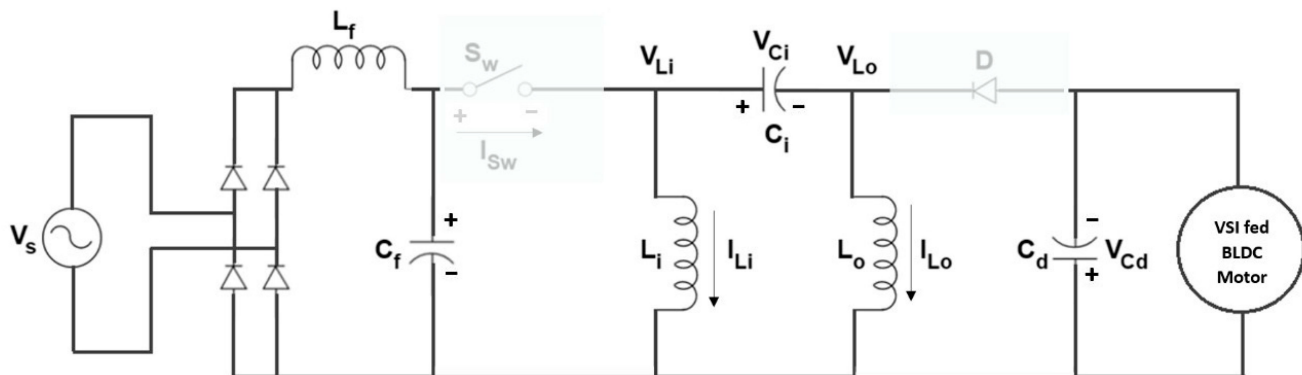


**Figure 10.** Mode 4 of the improved zeta converter.

## 6. Control of Proposed BLDC Drive

The control of the modified zeta converter-fed BLDC is divided into two parts as follows.

### 6.1. Control of PFC Modified Zeta Converter

The front-end PFC converter, which produces the PWM pulses for the PFC converter switch for DC-link voltage control, is controlled using a voltage follower strategy. For the PFC zeta converter running in DICM, a single voltage control loop (voltage follower technique) is used. A reference DC-link voltage  $V_{dc}^*$  is considered.

$$V_{dc}^* = K_v \times \omega^* \quad (3)$$

where  $\omega^*$  is the reference speed and  $K_v$  is the motor voltage constant.

DC-link reference voltage  $V_{dc}^*$  and detected DC-link voltage  $U_d$  can be compared to produce voltage error signal  $V_e$ . The proportional–integral (PI) controller receives this error voltage signal ( $V_e$ ) in order to produce a controlled voltage,  $V_c$ . Finally, the output of the voltage controller,  $V_c$ , is compared with a high-frequency saw-tooth signal ( $M_d$ ) to generate the PWM pulses as follows:

$$\begin{cases} \text{if } M_d(t) < V_c(t), \text{ then } S_w = \text{ON} \\ \text{if } M_d(t) \geq V_c(t), \text{ then } S_w = \text{OFF} \end{cases} \quad (4)$$

where  $S_w$  represents the switching signals of the PFC modified zeta converter.

### 6.2. Control of BLDC Motor for Torque Ripple Minimization

The voltage source inverter must be switched precisely during the electronic commutation of a BLDC motor. To locate the rotor within a  $120^\circ$  span, Hall effect position sensors are used. Due to the stator and rotor magnetic field interaction, torque ripples in BLDC motors occur. These interactions generate a “ripple” effect in the motor’s torque curve, which results in variations in its power output. The timing and accuracy of the commutation process may also cause torque ripples for one reason or another. If the current is not switched at precisely the right time, the magnetic field may not be properly aligned, leading to variations in the torque output. The main reason behind the ripple formation is that the commutation between two phases cannot be completed simultaneously. It is possible for three cases to occur when considering stator currents and the maximum value of the back-emf,  $E$ .

Case 1: If  $U_d$  is smaller than  $E$ , the commutation between the two phases cannot be completed simultaneously, i.e., the motor speed is higher than a specific value, and as a result,  $i_c$  does not reach its steady state value when  $i_a$  is zero. This can be seen in Figure 11a.

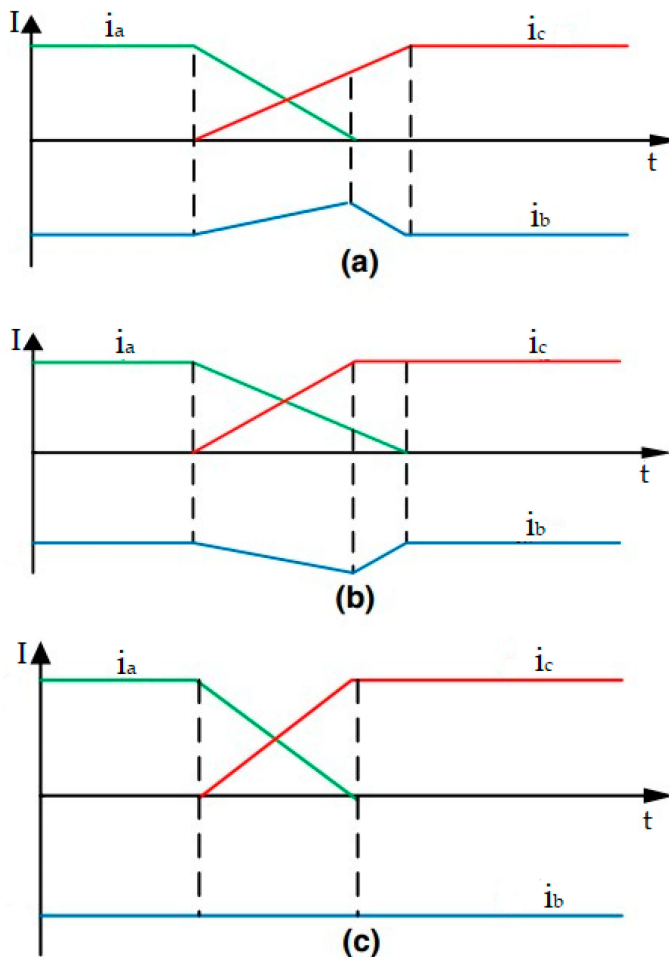


**Figure 11.** Different cases of commutation. (a) Negative Torque Ripple (b) Positive Torque Ripple (c) Zero Torque ripple.

Case 2: If  $U_d$  is greater than  $E$ , the motor cannot commute between the two phases at the same rate, and, as shown in Figure 11b,  $i_c$  achieves its constant state value before  $i_a$  reaches zero.

Case 3: If  $U_d$  and  $E$  are equal, the commutation between them can be finished simultaneously. If this occurs, the motor will run at a specific speed, causing  $i_c$  to attain its steady-state value just as  $i_a$  drops to zero, as shown in Figure 11c.

The amount of current in the non-commutating phase can be increased, decreased, or held constant. Thus, during commutation, the non-commutating phase has a positive slope at slower speeds and a negative slope at faster speeds. As a result, this slope is adjusted during commutation by injecting PWM pulses using the bilateral modulation scheme of PWM-ON-PWM. In this manner, the torque ripple brought on by the commutation current during the commutation period will be eliminated.

#### 6.2.1. Estimation of Duty Cycle for the PWM-ON-PWM Scheme

The main cause of torque ripples is commutation. For example, consider the region from 0 to  $\pi/2$ . As shown in Figure 12, the back-emf and current will be

$$\left\{ \begin{array}{l} e_a = E \\ e_b = E \\ e_c = -E \end{array} \right. \quad (5)$$

$$i_a = -i_c \text{ and } i_b = 0 \quad (6)$$

By substituting (5) and (6) into (2), the torque will be

$$T_e = \frac{-(2Ei_c)}{\omega} \quad (7)$$

From (7), it is clear that the torque is proportional to the non-commutation phase current during commutation, i.e., the commutation torque ripple can be eliminated by keeping the non-commutation phase current constant during the time of commutation.

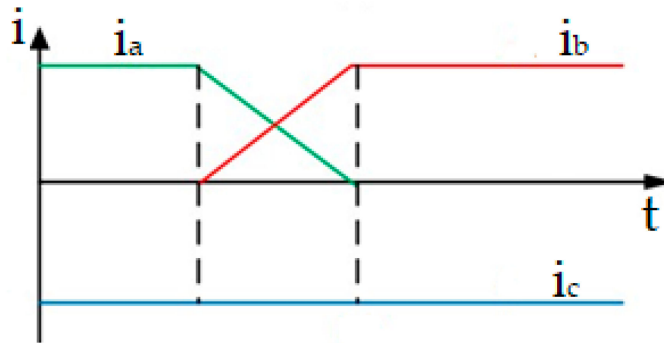


**Figure 12.** Ideal current commutation of BLDC motor.

The following is an analysis of the commutation process. For the analysis, overlapping commutation was suggested, which would control the PWM duty cycle in order to control the commutation torque ripple. Assuming that  $S_1$  was switched OFF and  $S_2$  was switched ON during a specific commutation procedure at the time the current is transferred from phase A to phase B,  $S_3$  is then chopped. For analysis, overlapping commutation was suggested, which would control the PWM duty cycle to control the commutation torque ripple. The three-phase voltage equations are, therefore:

$$V_a = D \times U_d = Ri_a + L \frac{di_a}{dt} + e_a + U_n \quad (8)$$

$$V_b = U_d = Ri_b + L \frac{di_b}{dt} + e_b + U_n \quad (9)$$

$$V_c = (1 - D)U_d = Ri_c + L \frac{di_c}{dt} + e_c + U_n \quad (10)$$

From the above three equations, the neutral voltage  $U_n$  can be obtained as

$$U_n = \frac{2U_d - e_a - e_b - e_c}{3} \quad (11)$$

The values 1 and 0 signify turning the switch on and off, respectively, while D stands for the switching function. In each PWM carrier cycle, S maintains a value of 1 during DT and a value of 0 during (1-D) T, where D is the PWM duty ratio.

Substituting (11) into (8), (9), and (10) the differential equations of the phase current become:

$$L \frac{di_a}{dt} = D \times U_d - e_a - U_n = \frac{(3D - 2)U_d + e_a + e_c - 2e_b}{3} = V_{a1} \quad (12)$$

$$Ri_b + L \frac{di_b}{dt} = U_d - e_b - U_n = \frac{U_d + e_a + e_c - 2e_b}{3} = V_{b1} \quad (13)$$

By considering the initial conditions (at  $t = 0$ )  $i_a = I$ ,  $i_b = 0$ ,  $i_c = -I$ ,

$$i_a = \frac{U_{a1}}{R} + \left( I - \frac{U_{a1}}{R} \right) e^{-(\frac{R}{L})t} \quad (14)$$

$$i_b = \frac{V_{b1}}{R} - \frac{V_{b1}}{R} e^{-(\frac{R}{L})t} = \frac{V_{b1}}{R} \left(1 - e^{-(\frac{R}{L})t}\right) \quad (15)$$

The first term can be described as  $e^{-(\frac{R}{L})t} = 1 - \left(\frac{R}{L}\right)t$ . Substituting it into (14) and (15), the time  $t_a$  when  $i_a$  decreases from 1 to 0 and the time  $t_b$  when  $i_b$  increases from 0 to 1 can be explained as

$$t_a = \frac{3IL}{2e_a - e_b - e_c + (3D - 2) \times U_d} \quad (16)$$

$$t_b = \frac{3IL}{U_d + e_a + e_c - 2e_b} \quad (17)$$

Thus, the duty cycle of PWM can therefore be stated as:

$$D(k) = 1 - \frac{e_a(k) + e_b(k) - 2e_c(k)}{3U_d} \quad (18)$$

The duty ratio given in Equation (16) is used for providing gate pulses to the switches of the inverter.

#### 6.2.2. Pulse Width Modulation Scheme: Digital Logic of PWM-ON-PWM Scheme

A suitable switching of VSI is one of the important parts of the electronic commutation of the BLDC motor, drawing a symmetrical dc current for  $120^\circ$  from the DC-link capacitor and placing it in the middle of each phase. Rotor position sensing over a span of  $120^\circ$  is accomplished using Hall effect position sensors. The applied DC-link voltage, back electromotive forces, resistance, and self- and mutual inductance of the stator windings all affect how much current flows through them. Six switching pulses are needed for the proper switching of the inverter. Two switches per phase are present. The back emf signal and current/decoded hall sensor signals are considered for the implementation of the PWM pattern. For phase A, current  $i_a$  and back-emf  $e_b$  and  $e_c$  are considered; similarly, for phase B, current  $i_b$  and back-emf  $e_c$  and  $e_a$  are studied; and for phase C, current  $i_c$  and back-emf  $e_b$  and  $e_a$  are considered. In the PWM\_ON\_PWM pattern, for the first and last  $30^\circ$ , PWM mode is used, and for the middle  $60^\circ$ , the constant turn-on mode is used. In order to implement this, logical operations were mainly used. For the implementation of the first  $30^\circ$  of phase A, the region of  $i_a = 1$  and  $e_c \geq 0$  was considered and the first  $30^\circ$  were developed. The region of  $i_a = 1$  and  $e_b \geq 0$  was considered to develop the last  $30^\circ$ . By providing OR operation, a combination of the first and last  $30^\circ$  will occur. For the next step, XOR operation of this developed region with  $i_a = 1$  will allow a constant  $60^\circ$  region to develop. Then, by using AND operation, the pulses developed by using the duty ratio as per Equation (18) with the combination of first and last  $30^\circ$  will generate a combination of the first and last  $30^\circ$  PWM pulses. For the final stage, the OR operation is provided with the XOR output, and the combination of the first and last  $30^\circ$  PWM pulses will generate the PWM-ON-PWM pattern. Similar operations are used for the next two phases, and these, correspondingly, will generate the PWM-ON-PWM pattern. The digital logic of the PWM-ON-PWM scheme and a complete scheme of implementation using MATLAB are shown in Figure 13.

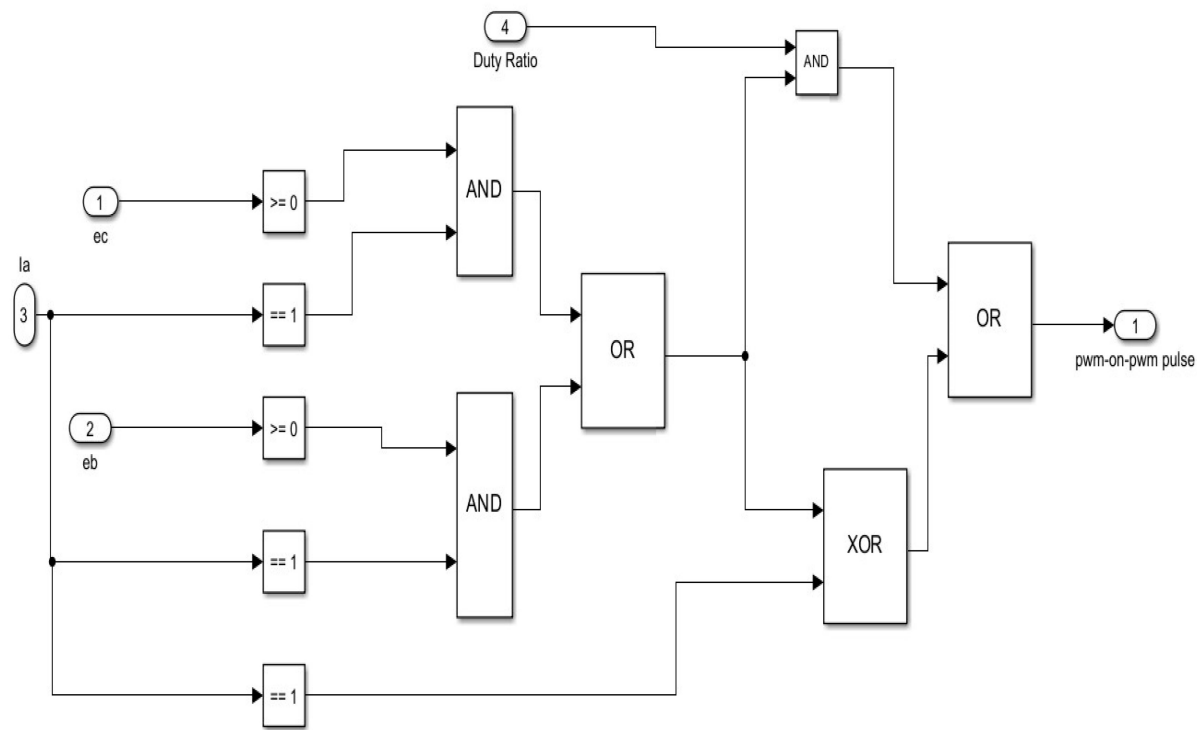


**Figure 13.** Digital logic of the PWM-ON-PWM scheme.

## 7. Results and Analysis

With the aid of the MATLAB/Simulink, the proposed system is illustrated with ideal models of all the elements. Design factors for the employed zeta converter and BLDC motor are mentioned in Tables 1 and 2, respectively. The framework of the proposed scheme to achieve the power factor correction and torque ripple minimization is shown in Figure 14.

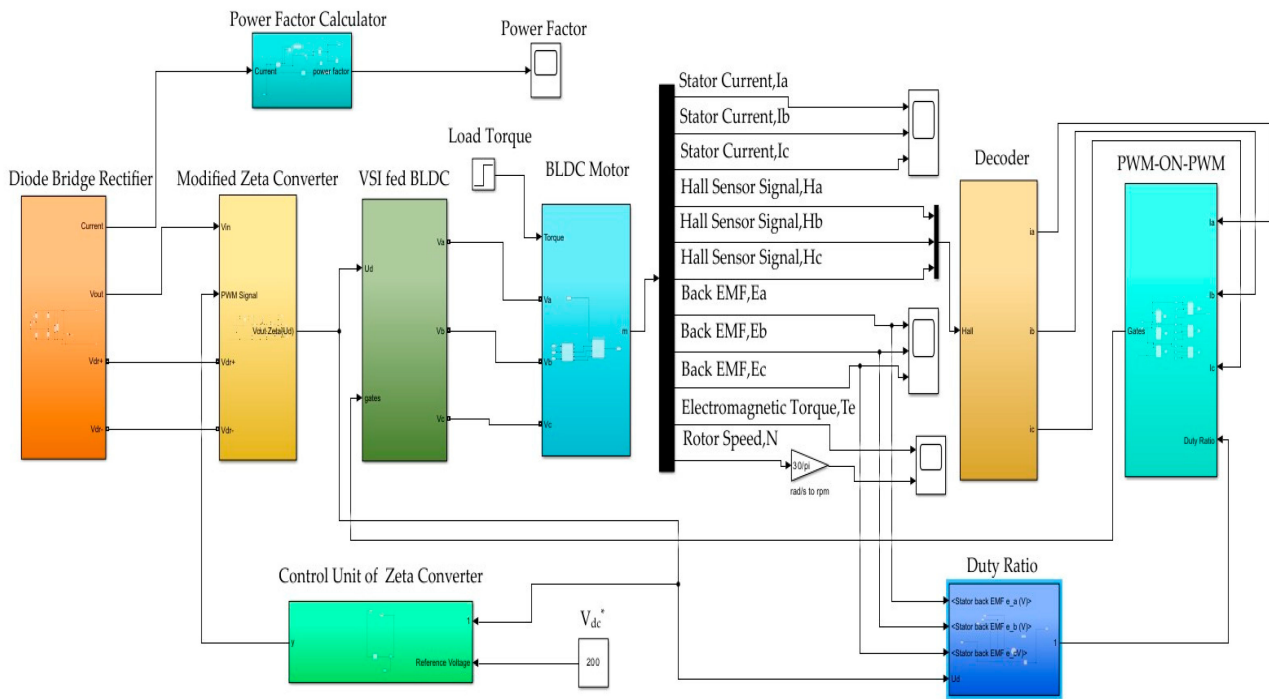
**Table 1.** Parameters of the zeta converter.

Symbol	Quantity	Value of Parameter
$V_{in}$	Input Voltage	100 V
$U_d$	Output Voltage	200 V
$L_i$	Input Inductance	3.3 mH
$L_o$	Output Inductance	70 mH
$C_i$	Intermediate Capacitance	0.66 $\mu$ F
$C_d$	Output Capacitance	2200 $\mu$ F
$S_w$	Switching Frequency	10 kHz

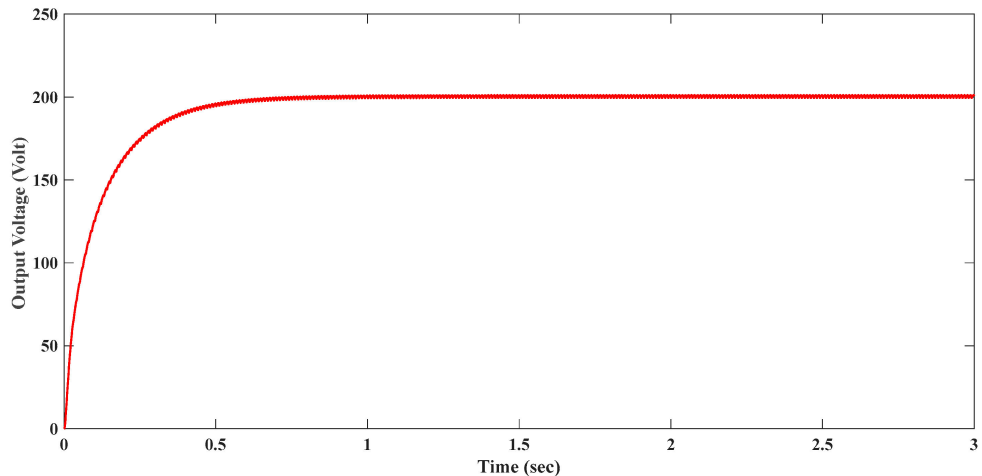
**Table 2.** Parameters of the BLDC motor.

Symbol	Quantity	Value of Parameter
$U_d$	Input Voltage	200 V
$J$	Moment of Inertia	0.12 $\text{Kg m}^2$
$B$	Friction Coefficient	0.005 Nm/rad/sec
$K_e$	Back-emf Constant	0.07 V/rad/sec
$R$	Resistance per phase	0.2 $\Omega$
$L$	Inductance per phase	8.5 mH
$P$	Number of pole pairs	4
$T$	Torque	2 Nm

This model mainly focuses on improving the power factor of the BLDC motor drive using the modified zeta converter. In this model, the modified zeta converter is designed to produce an output voltage of 200 V, which is demonstrated in Figure 15.



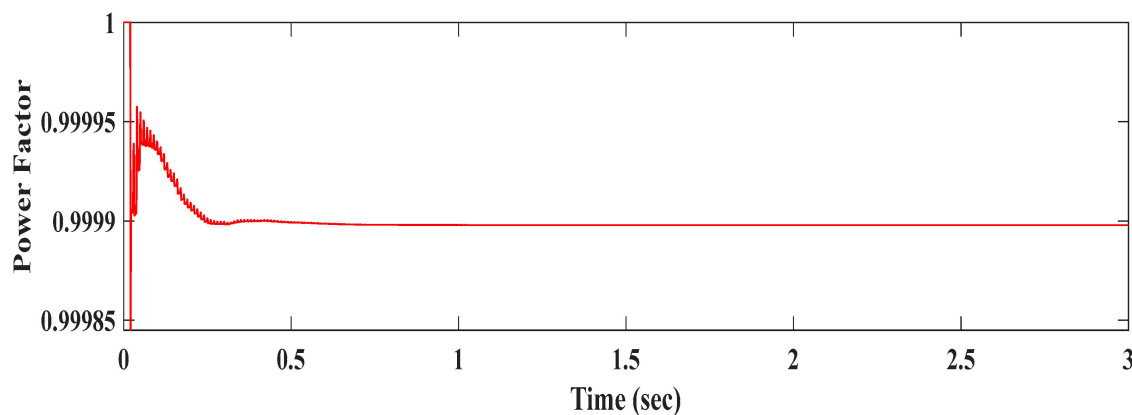
**Figure 14.** Simulation model of the proposed system.



**Figure 15.** Output voltage of zeta converter.

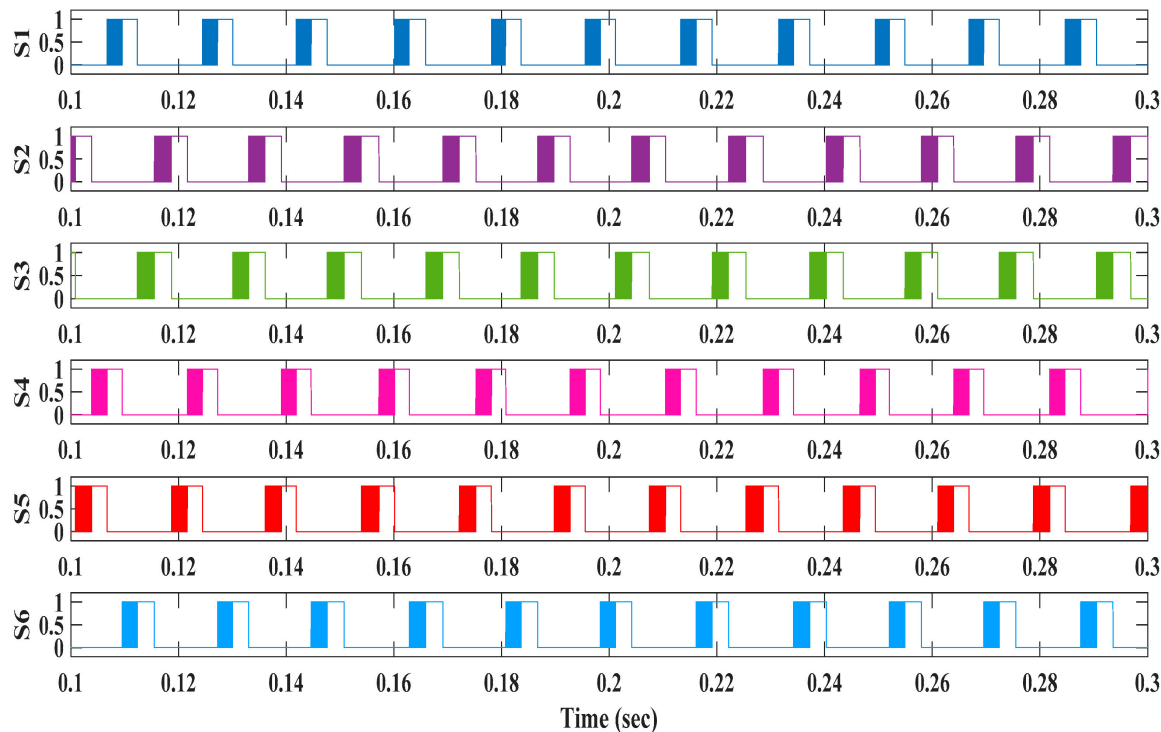
In a BLDC drive that does not incorporate a zeta converter, the rectifier stage commonly employs a diode bridge configuration to convert the AC input voltage into a pulsating DC voltage. This pulsating DC voltage is subsequently fed into a voltage source inverter, which generates the three-phase voltage waveforms necessary for driving the BLDC motor. However, the diode bridge rectifier operates by drawing current from the AC supply in short pulses, resulting in a distorted input current waveform characterized by a low power factor. Introducing a zeta converter into the rectifier stage of the BLDC drive can improve the power factor. The zeta converter could regulate the input current, which would allow it to determine the shape of the input voltage and reduce its harmonics in a way that would allow for an improved power factor through control of the switch timing and the duty cycle.

Figure 16 shows the power factor obtained from the simulated model. From Figure 16, it is clear that the power factor value is 0.9999, which is approximately equal to unity and demonstrates the UPF operation of the modified zeta converter-fed BLDC drive.



**Figure 16.** Power factor of the BLDC drive.

PWM-ON-PWM is the suggested technique to deal with the commutation current ripple in the commutation zone and the freewheeling diode in the non-commutation zone. To validate the results of the PWM-ON-PWM scheme, a comparison using a PWM-ON scheme is also introduced. The PWM-ON technique is not able to reduce the torque ripple at the end of commutation or the ON-PWM technique at the beginning of commutation. The PWM-ON-PWM control strategy is suggested for the concurrent execution of both tasks. As a result, the PWM-ON-PWM scheme can reduce the freewheeling diode current in the first and last  $30^\circ$  of commutation. To validate the results, the PWM-ON scheme is also implemented. The results of the simulated model are depicted below. Figure 17 shows the PWM-ON pulses exhibited by the MOSFET switches of the BLDC drive.



**Figure 17.** Simulated waveform of the PWM-ON pattern.

The simulated stator current waveforms of the BLDC drive using the PWM\_ON scheme are shown in Figure 18.

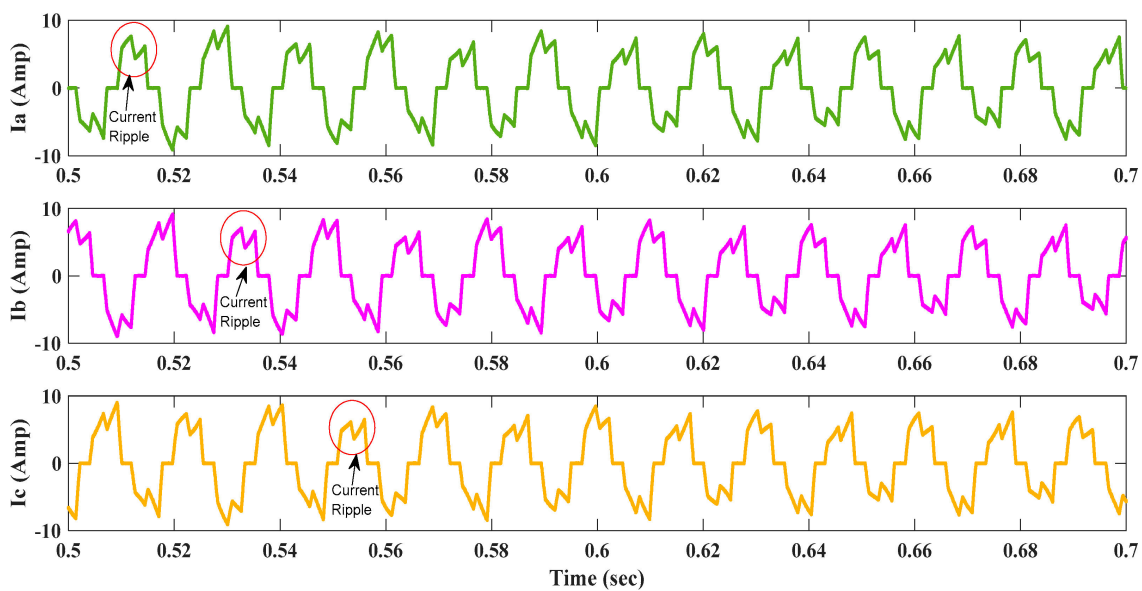


**Figure 18.** Simulated waveform of the stator current using the PWM-ON switching scheme.

It is important to note that the freewheeling diode enters the scene at the last  $30^\circ$  of commutation in Figure 18. PWM-ON approaches have the current ripple overlaid on the stator current in the non-commutation zone because of the diode freewheeling of the inactive phase.

A load torque of 2 Nm is applied for 3 s, and the performance is analyzed. A simulated waveform of the BLDC drive using the PWM-ON scheme is shown in Figure 19, and the expanded view is also included.

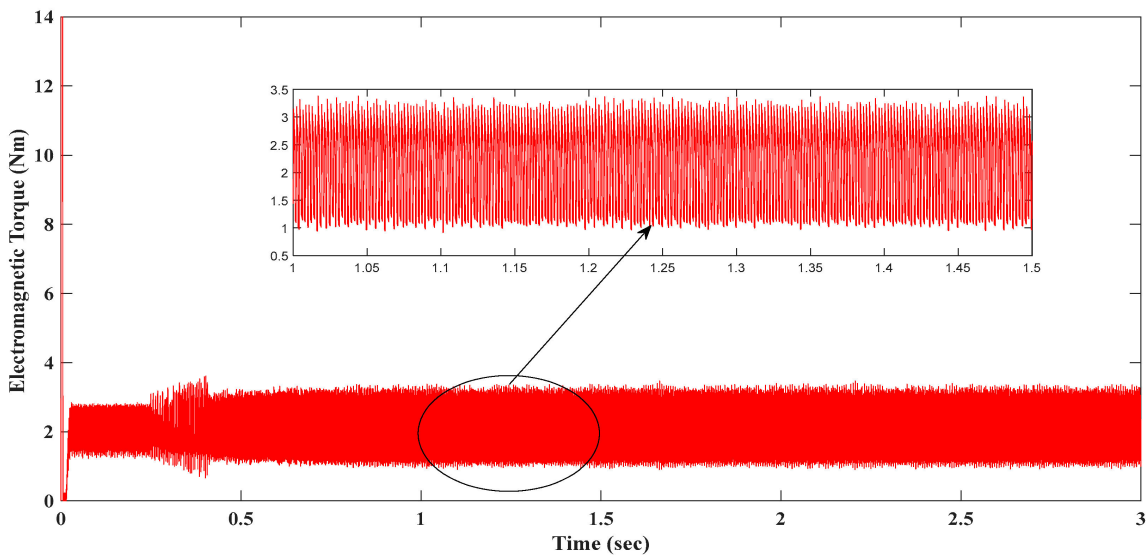


**Figure 19.** Electromagnetic torque using the PWM-ON scheme.

Torque ripples in the BLDC drive are calculated by

$$\text{Torque Ripple (\%)} = \frac{T_{max} - T_{avg}}{T_{avg}} * 100 \quad (19)$$

From the expanded figure, it is clear that torque ripples of about 58.9% are present in the drive using the PWM-ON scheme.

The details of BLDC motor operation using the PWM-ON-PWM scheme are given below. PWM-ON-PWM pulses are used to attain torque ripple minimization in the BLDC drive, fed to the MOSFET's of VSI. In the PWM-ON-PWM pattern, for the first and last  $30^\circ$ , PWM pulses are provided, and for the middle  $60^\circ$ , a constant turn-on scheme is followed. The simulated waveform of the PWM-ON-PWM pattern is shown in Figure 20.

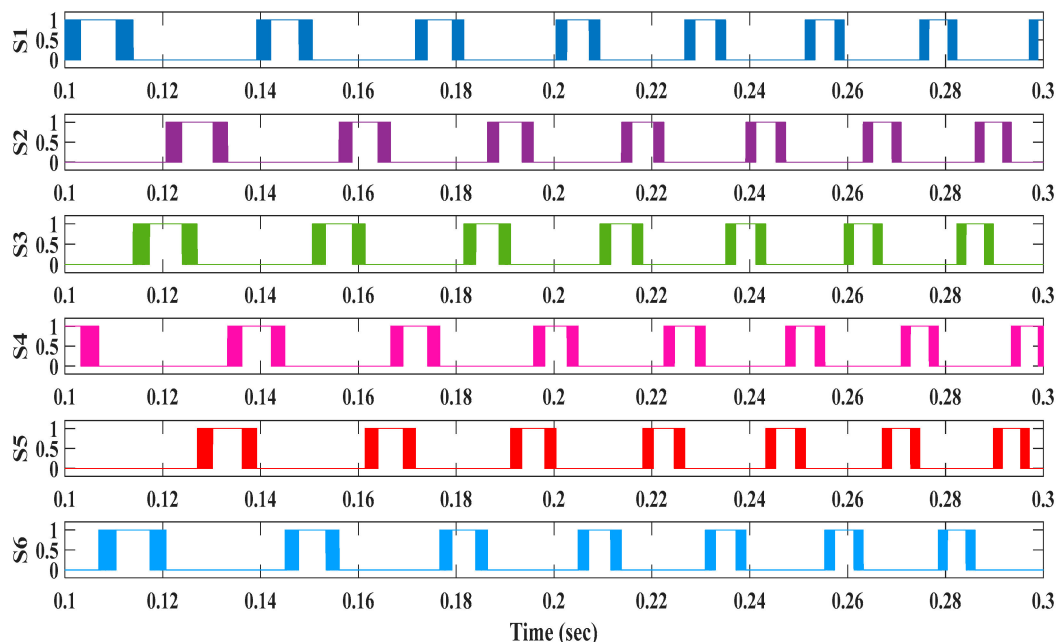


**Figure 20.** Simulated waveform of the PWM-ON-PWM pattern.

Using the same parameters, the stator currents and back emf of the BLDC motor based on the PWM-ON-PWM technique and the zeta converter are depicted in Figures 21 and 22. It is crucial to remember that PWM pulses are offered in both the first and last  $30^\circ$  of the commutations, which completely eliminates the freewheeling action of the diode and develops a ripple-free stator current waveform of a constant amplitude with no distortion.

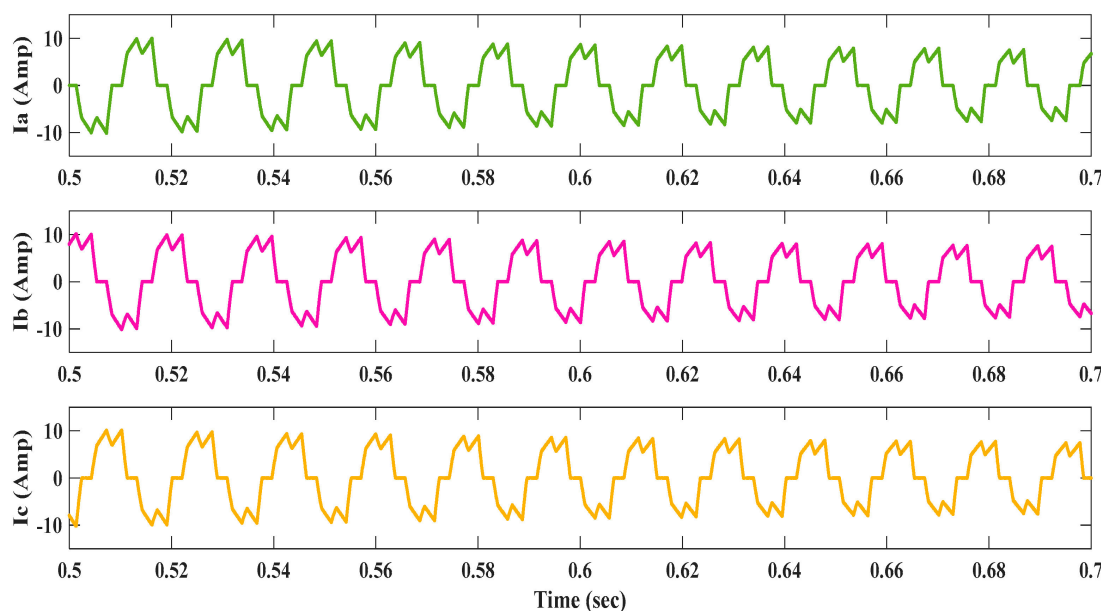


**Figure 21.** Simulated waveform of the stator current using the PWM-ON-PWM switching scheme.

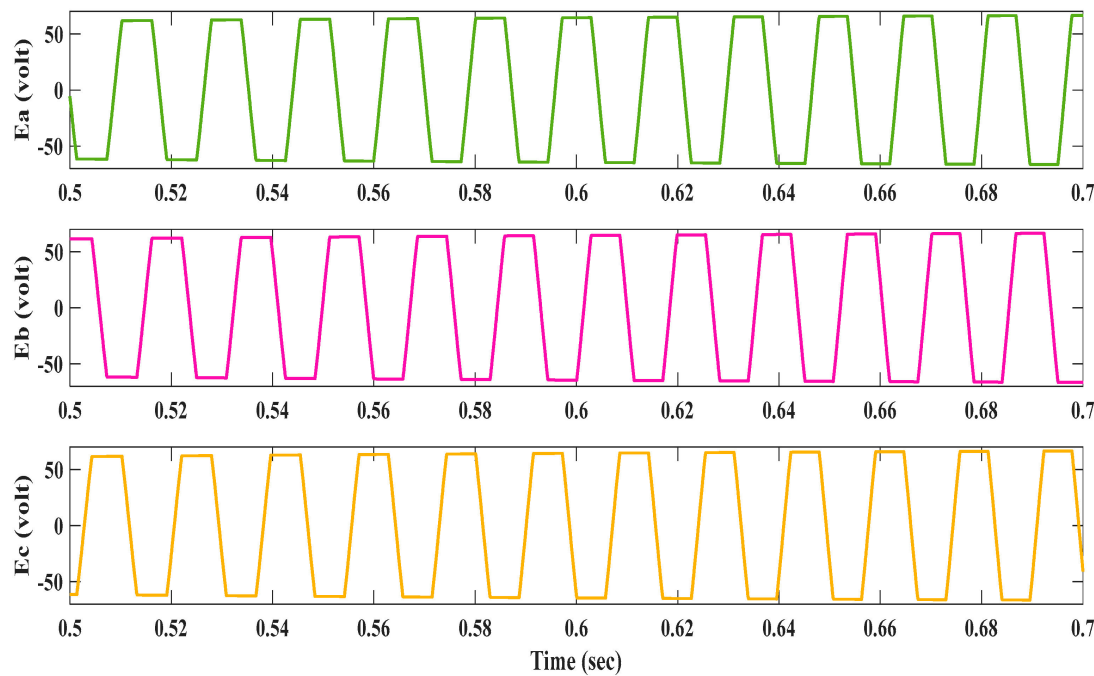


**Figure 22.** Simulated waveform of the back emf using the PWM-ON-PWM switching scheme.

The trapezoidal back-emf of BLDC drive using the PWM-ON\_PWM scheme is illustrated in Figure 22. To analyze the feasibility of the proposed PWM-ON-PWM switching scheme, a load torque of 2 Nm was applied for 3 s and the performance was analyzed. A simulated waveform using the PWM-ON-PWM scheme is shown in Figure 23. The expanded view is also depicted.

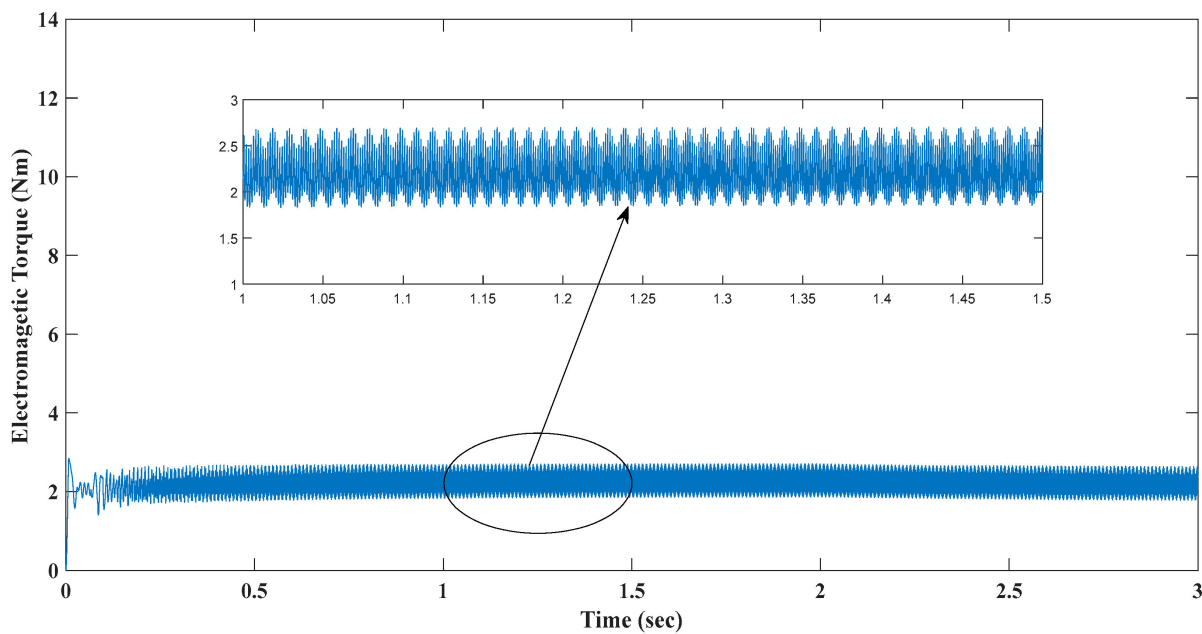


**Figure 23.** Electromagnetic torque using the PWM-ON-PWM switching scheme.

By comparison with the PWM-ON scheme, it becomes clear that the torque ripples in the BLDC drive using PWM-ON-PWM were less as compared to PWM-ON. With the proposed scheme, the torque ripple in the BLDC drive was only 24.7%.

PWM-ON-PWM mode reduces the torque ripple caused by the current during the time of commutation. For showing the variation in torque, expanded waveforms using the PWM-ON and PWM-ON-PWM patterns are depicted in Figure 24. From Figure 24, it is clear that the torque ripples were less in the PWM-ON-PWM scheme as compared to the PWM-ON scheme. The PWM-ON-PWM was able to reduce the torque ripple by 34.2%.

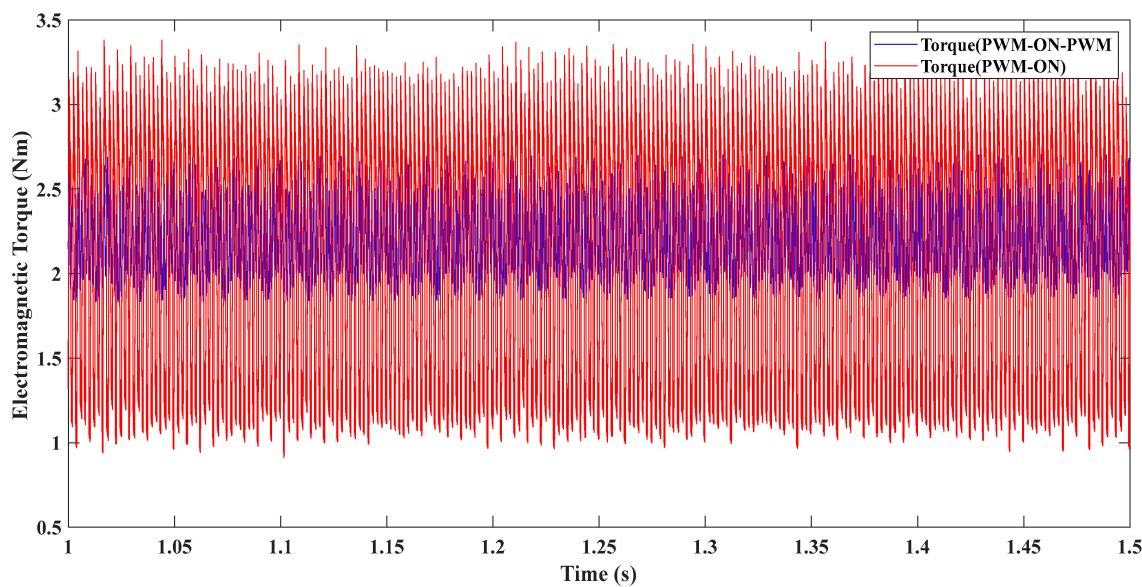


**Figure 24.** Electromagnetic torque using the PWM-ON-PWM and PWM-ON patterns.

The proposed system can be used for both constant- and variable-speed applications. For a reference speed of 1200 rpm, the motor followed the reference speed quickly, as shown in Figure 25. Also, when loaded, the machine was capable of supplying the required load torque demand. Thus, it is very evident from the result that the drive is doing well. The outcomes clearly demonstrate the viability of the suggested approach.

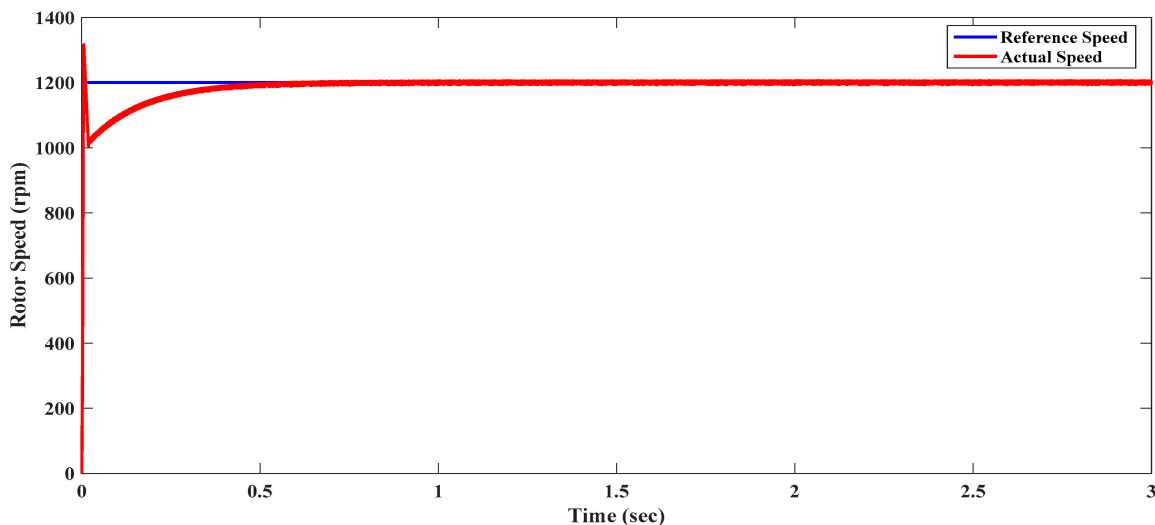


**Figure 25.** Speed response of the BLDC drive using the PWM-ON-PWM pattern.

The ability to control motor speed allows for optimized performance, energy efficiency, and precise operation in diverse applications. BLDC drives with variable speed capabilities find extensive applications in electric vehicles, HVAC systems, industrial automation, aerospace, renewable energy, robotics, and medical equipment. The proposed drive is

also applicable to variable speed applications, and the operation of the drive for variable driving cycles is shown in Figure 26.

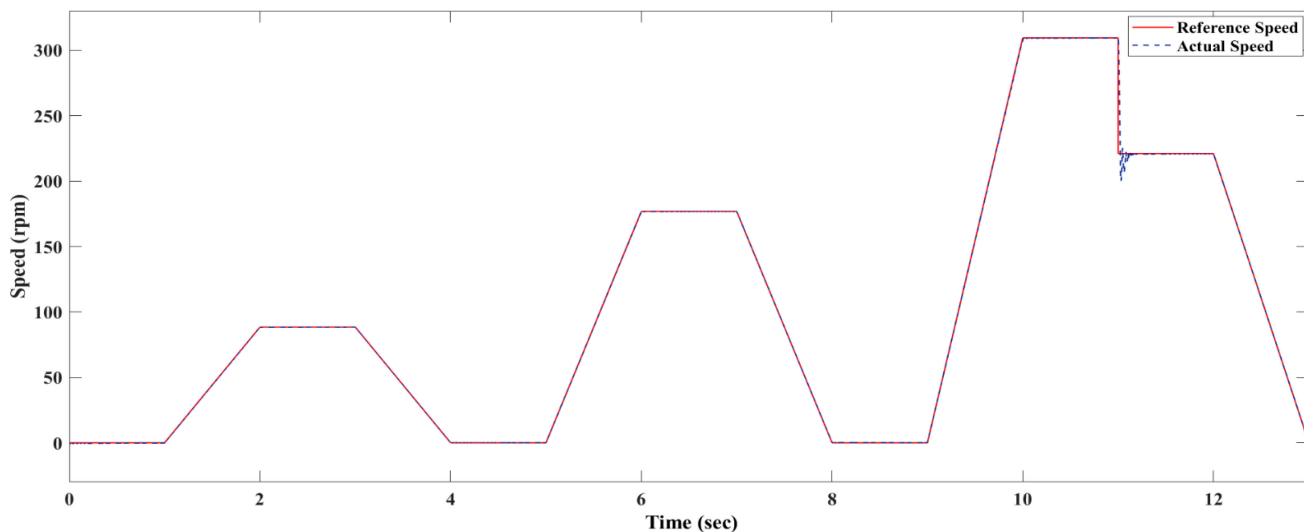


**Figure 26.** Variable speed response of the BLDC drive using the PWM-ON-PWM pattern.

## 8. Conclusions

The PWM-ON-PWM switching logic was proposed to reduce the torque ripples in the BLDC drive, and the improved zeta converter to improve the power factor. The PFC-modified zeta converter offers a good power factor correction capacity. With a power factor of 0.9999, the PFC-modified zeta converter's topology outperforms the topology explained in [10]. A power factor correction zeta converter-driven BLDC motor drive was shown to have a wide range of speed control with the unit power factor at the supply mains. The modified zeta converter was used to control the DC-link voltage of VSI, which in turn controlled the BLDC motor's speed. It is possible to use the drive for both constant- and variable-speed applications. Additionally, a comparative study was presented using the PWM-ON and PWM-ON-PWM switching strategy. It was observed that the PWM-ON switching offered 58.9% ripples, whereas the proposed method offered only 24.7% of the torque ripples. The PWM-ON-PWM method was able to reduce the torque ripples by 34.2%, which is a lesser result than that mentioned in [23]. The effectiveness of the proposed strategy was illustrated by simulation. The combination of these techniques offers a better power factor and better torque ripple minimization in BLDC drives, thus having a positive impact on both industrial and energy-saving efforts.

## 9. Future Works

Future work will consider the practical grid interfaced solar water pumping system, which includes a PV panel, an improved zeta converter, and a voltage source inverter of a BLDC motor using the PWM-ON-PWM scheme with a new topology for a bidirectional converter. The methodology in the manuscript will be incorporated into the future work in a practical way. Integration with the grid will be a significant milestone in terms of enhancing the solar water pumping system's functionality. By enabling bidirectional power flow, the system can efficiently utilize surplus solar energy, which can be injected back into the grid, ensuring an environmentally friendly approach and potential revenue generation through net metering schemes. This switching strategy can be used in situations where torque ripple minimization is crucial.

**Author Contributions:** Conceptualization, G.K. and M.S.; methodology, G.K.; software, G.K.; validation, M.S. and S.V.; formal analysis, M.S.; investigation, G.K.; resources, G.K. and M.S.; data curation, G.K.; writing—original draft preparation, G.K.; writing—review and editing, M.S. and S.V.; visualization, G.K.; supervision, M.S. and S.V.; project administration, M.S. All authors have read and agreed to the published version of the manuscript.

**Funding:** This research received no external funding.

**Institutional Review Board Statement:** Not applicable.

**Informed Consent Statement:** Not applicable.

**Data Availability Statement:** Not applicable.

**Acknowledgments:** The authors are grateful for the administrative and technical support from the Ariel University, Ariel, Israel, and Jyothi Engineering College, Kerala, India.

**Conflicts of Interest:** The authors declare no conflict of interest.

## References

1. Mohanraj, D.; Aruldavid, R.; Verma, R.; Sathiyasekar, K.; Barnawi, A.B.; Chokkalingam, B.; Mihet-Popa, L. A Review of BLDC Motor: State of Art, Advanced Control Techniques, and Applications. *IEEE Access* **2022**, *10*, 54833–54869. [[CrossRef](#)]
2. Kumar, N.S.; Chandrasekaran, G.; Thangavel, J.; Vanchinathan, K.; Chandrasekaran, G.; Priyadarshi, N.; Bhaskar, M.S.; Hussien, M.G.; El-Sousy, F.F.M.; Ali, M.M. A Novel Design Methodology and Numerical Simulation of BLDC Motor for Power Loss Reduction. *Appl. Sci.* **2022**, *12*, 10596. [[CrossRef](#)]
3. Saha, S.; Modal, S.; Chattopadhyay, M.; Mukherjee, M. A Scheme for Torque Ripple Minimization in BLDC Drive Using Two-Inductor Boost Converter. In Proceedings of the 2022 IEEE International Conference of Electron Devices Society Kolkata Chapter, EDKON, Kolkata, India, 26–27 November 2022; pp. 69–74. [[CrossRef](#)]
4. Singh, B.; Chandra, A.; Al-Haddad, K.; Pandey, A.; Kothari, D. A review of single-phase improved power quality AC~DC converters. *IEEE Trans. Ind. Electron.* **2003**, *50*, 962–981. [[CrossRef](#)]
5. Singh, B.; Bist, V. Power factor correction (PFC) converters feeding brushless DC motor drive. *Int. J. Eng. Sci. Technol.* **2016**, *7*, 65–75. [[CrossRef](#)]
6. Singh, B.; Singh, S. Single-phase power factor controller topologies for permanent magnet brushless D.C. motor drives. *IET Power Electron.* **2010**, *3*, 147–175. [[CrossRef](#)]
7. Wu, C.-H.; Tzou, Y.-Y. Digital control strategy for efficiency optimization of a BLDC motor driver with VOPFC. In Proceedings of the 2009 IEEE Energy Conversion Congress and Exposition, San Jose, CA, USA, 20–24 September 2009; pp. 2528–2534. [[CrossRef](#)]
8. Singh, B.; Bist, V. Power quality improvements in a zeta converter for brushless DC motor drives. *IET Sci. Meas. Technol.* **2015**, *9*, 351–361. [[CrossRef](#)]
9. Gopalarathnam, T.; Toliat, H. A new topology for unipolar brushless DC motor drive with high power factor. *IEEE Trans. Power Electron.* **2003**, *18*, 1397–1404. [[CrossRef](#)]
10. Bin, L.; Abdeen, Z.U.; Abrar, M.; Muheet, H.A.; Shahzad, M.; Zulfiqar, M.; Hussain, M.M. A novel approach to design of a power factor correction and total harmonic distortion reduction-based BLDC motor drive. *Front. Energy Res.* **2023**, *10*, 96389. [[CrossRef](#)]
11. Glowacz, A. Thermographic Fault Diagnosis of Ventilation in BLDC Motors. *Sensors* **2021**, *21*, 7245. [[CrossRef](#)]
12. Ali, J.A.; Hannan, M.; Mohamed, A. A Novel Quantum-Behaved Lightning Search Algorithm Approach to Improve the Fuzzy Logic Speed Controller for an Induction Motor Drive. *Energies* **2015**, *8*, 13112–13136. [[CrossRef](#)]
13. Huang, C.-L.; Wu, C.-J.; Yang, S.-C. Full-Region Sensorless BLDC Drive for Permanent Magnet Motor Using Pulse Amplitude Modulation with DC Current Sensing. *IEEE Trans. Ind. Electron.* **2021**, *68*, 11234–11244. [[CrossRef](#)]
14. Shchur, I.; Lis, M.; Biletskyi, Y. Passivity-Based Control of Water Pumping System Using BLDC Motor Drive Fed by Solar PV Array with Battery Storage System. *Energies* **2021**, *14*, 8184. [[CrossRef](#)]
15. Gu, C.; Wang, X.; Shi, X.; Deng, Z. A PLL-Based Novel Commutation Correction Strategy for a High-Speed Brushless DC Motor Sensorless Drive System. *IEEE Trans. Ind. Electron.* **2018**, *65*, 3752–3762. [[CrossRef](#)]
16. Shchur, I.; Jancarczyk, D. Electromagnetic Torque Ripple in Multiple Three-Phase Brushless DC Motors for Electric Vehicles. *Electronics* **2021**, *10*, 3097. [[CrossRef](#)]
17. Yao, X.; Lu, G.; Zhao, J.; Lin, H. Torque Ripple Minimization in Brushless DC Motor with Optimal Current Vector Control Technique. In Proceedings of the 2018 Chinese Automation Congress (CAC), Xi'an, China, 30 November–2 December 2018; pp. 2524–2529. [[CrossRef](#)]
18. Viswanathan, V.; Jeevananthan, S. Approach for Torque Ripple Reduction for Brushless DC Motor Based on Three-Level Neutral-Point-Clamped Inverter with DC-DC Converter. *IET Power Electron.* **2015**, *8*, 47–55. [[CrossRef](#)]
19. Viswanathan, V.; Seenithangom, J. Commutation Torque Ripple Reduction in the BLDC Motor Using Modified SEPIC and Three-Level NPC Inverter. *IEEE Trans. Power Electron.* **2018**, *33*, 535–546. [[CrossRef](#)]
20. Kumar, D.; Gupta, R.A.; Tiwari, H. Front-end zeta converter based BLDCM drive for efficient reduction of commutation current ripple using notch-filter. *Int. Trans. Electr. Energy Syst.* **2020**, *30*, e12508. [[CrossRef](#)]

21. Kumar, D.; Gupta, R.A.; Tiwari, H. A Novel High Voltage Gain SEPIC Converter Based on Hybrid Split-Inductor for Renewable Application. *IETE J. Res.* **2020**, *68*, 3457–3473. [[CrossRef](#)]
22. Azab, M. Comparative Study of BLDC Motor Drives with Different Approaches: FCS-Model Predictive Control and Hysteresis Current Control. *World Electr. Veh. J.* **2022**, *13*, 112. [[CrossRef](#)]
23. Kumar, D.; Choudhary, S.D.; Tabrez; Ayob, A.; Lipu, M.S.H. Model Antiseptic Control Scheme to Torque Ripple Mitigation for DC-DC Converter-Based BLDC Motor Drives. *Energies* **2022**, *15*, 7823. [[CrossRef](#)]
24. Gamazo-Real, J.C.; Vázquez-Sánchez, E.; Gómez-Gil, J. Position and Speed Control of Brushless DC Motors Using Sensorless Techniques and Application Trends. *Sensors* **2010**, *10*, 6901–6947. [[CrossRef](#)] [[PubMed](#)]

**Disclaimer/Publisher’s Note:** The statements, opinions and data contained in all publications are solely those of the individual author(s) and contributor(s) and not of MDPI and/or the editor(s). MDPI and/or the editor(s) disclaim responsibility for any injury to people or property resulting from any ideas, methods, instructions or products referred to in the content.